Shaking table testing of groin vaults made by 3D printers

Published Version:
Silvestri S., Baraccani S., Foti D., Ivorra S., Theodossopoulos D., Vacca V., et al. (2021). Shaking table testing of groin vaults made by 3D printers. SOIL DYNAMICS AND EARTHQUAKE ENGINEERING, 150, 1-18 [10.1016/j.soildyn.2021.106880].

Availability:
This version is available at: https://hdl.handle.net/11585/858980 since: 2022-02-15

Published:
DOI: http://doi.org/10.1016/j.soildyn.2021.106880

Shaking Table Testing of Groin Vaults made by 3D Printers

Stefano Silvestri[1], Simonetta Baraccani[1*], Dora Foti[2], Salvador Ivorra[3], Dimitris Theodossopoulos[4], Vitantonio Vacca[2], Jacqueline Ochoa Roman[1], Luca Cavallini[1], Elnaz Mokhtari[1], RoryWhite[5], Matt Dietz[5], George Mylonakis[5,6,7]

[1]*Department Department of Civil, Chemical, Environmental and Materials Engineering, University of Bologna, Bologna, Italy*

[2]*Department of Civil Engineering Sciences and Architecture, Technical University of Bari, Bari, Italy*

[3]*Department of Civil Engineering, University of Alicante, Alicante, Spain*

[4]*Edinburgh School of Architecture and Landscape Architecture, University of Edinburgh, Edinburgh, United Kingdom, UK*

[5]*Department of Civil Engineering, University of Bristol, Bristol, United Kingdom*

[6]*Department of Civil Infrastructure & Environmental Engineering, Khalifa University, U.A.E.*

[7]*Department of Civil & Environmental Engineering, University of California at Los Angeles (UCLA), U.S.A.*

**corresponding author*

Abstract

A novel experimental study of the seismic response of a 2 m x 2 m in plan - 0.7 m in height groin vault model, involving 266 tests conducted on the shaking table of EQUALS laboratory, University of Bristol, UK, is reported. The experimental rig consists of blocks formed by a 3D-printed plastic skin to provide stiffness and strength, filled with mortar. Dry joints between the voussoirs are formed for ease of testing and vault reconstruction. No investigations of this kind and size have been attempted in the past. Two support boundary conditions involving four lateral confinement modes, leading to various vault configurations, were tested. White-noise, sinusoidal and earthquake motions were imposed in one horizontal direction, with progressively increasing amplitude and different frequencies, up to collapse. The model exhibited a strongly non-linear behaviour, with decreasing fundamental frequency and increasing damping with increasing table acceleration. Failure mechanisms and collapse accelerations were found to mainly depend on base restraint conditions.

Keywords

Groin vault; 3D printer; Shaking table; Frequency; Damping; Collapse; Moveable springings

1 Introduction

Several types of historical masonry buildings are prone to earthquake damage, due to the presence of vulnerable elements such as vaulted roofing, irregular structural configurations (both in plan and elevation) and progressive structural weakening caused by aging and successive seismic events.

The analysis of damage in historical masonry churches has revealed different collapse mechanisms, associated with the local response of specific structural elements. In particular, observations following strong earthquakes suggest that out of all structural elements in this type of construction, the most vulnerable are masonry vaults [1], [2], [3]. Knowledge of the dynamic behaviour of these structures is fundamental for relevant analyses and effective interventions. However, the evaluation of seismic response of such systems is complex and depends on several factors including three-dimensional geometry, mechanical properties of the constituent materials, behaviour of the supporting elements (e.g., lateral walls and piers, buttresses) and joint construction quality.

Several studies are available in the literature on structural behaviour of masonry vaults. The use of limit analysis, introduced by Baker and Symonds and Neal for steel frames in the late 1940's and early1950's [4], [5], [6] and later extended by Heyman for masonry structures [7], [8], [9], provides fundamental insight into static/pseudo-static behaviour and the associated stability limits. Many experimental studies have investigated the structural behaviour of arches and vaults under horizontal actions, focusing particularly on dynamic response [10], [11], [12]. Other studies focused on displacement-controlled tests by applying widening and shortening displacements at the springings, mainly under static [13], [14], [15] or pseudo-static [16], [17], [18], [19] conditions, to explore the importance of the response of the supporting elements. In addition, computational methods such as the Finite Element Method (FEM) and Discrete Element Method (DEM) [20], [21], [22] have expanded our understanding of the behaviour of the particular structural type and geometry, but still without a satisfactory application in real problems. DEM, in particular, offers the possibility of modelling the interfaces and including the visible discontinuities when bricks separate, by simulating the structure as an assembly of distinct units (blocks). Nevertheless, it is fundamental to determine the relevant mechanical parameters to successfully model masonry. Despite the availability of a large volume of recent studies on the dynamic and seismic behaviour of arches [23], [24], [25] and of barrel and cross vaults [17], [22], [26], [27], [28], [29], experimental research is still needed the mechanics of groin pointed vaults.

This paper reports on a set of preliminary results from a shaking table campaign on a scaled model of a groin pointed vault, conducted at the Earthquake and Large Structures (EQUALS) Laboratory, University of Bristol, UK, under the auspices of a H2020 SERA project (SEBESMOVA3D) [30].
A 2m x 2m in-plan, 0.7 m tall vault model encompassing dry joints (i.e. unilateral joints with an interposed elastic gum layer) between the voussoirs, like many monumental structures in the Mediterranean, was built in an innovative way, with blocks made of a 3D-printed plastic material. The skin was filled with mortar to provide inertia and allow quick repetition of tests, carried out until collapse. This technique was used in earlier similar tests conducted on a small barrel vault at the "Laboratorio Salvati", Technical University of Bari, Italy [31], where modular blocks made of wood and stone with dry joints were employed to form innovative arches [32], [33]. A similar technique was adopted by Quinonez and co-workers [34] for a small-scale experimental investigation of collapse due to outward support displacements on two model domes (thickness of 17.3 mm and 32.8 mm, respectively) created from individual printed blocks. Further, Van Mele and co-workers [22] studied the collapse of a small-scale 3D-printed groin vault model (span of 150 mm and thickness of about 24.4 mm) under large support displacements. Shapiro et [12] used the 3D-printing technique to perform tests considering pseudo-static horizontal accelerations realised through tilting of the base of a groin vault composed of two barrel vaults (318 mm deep, 24 mm thick) and an angle of embrace of 110°. More recently, Rossi et al. [29] performed pseudo-static tests on a cross vault scaled model built by 3D printed plastic blocks with dry joints (span of 0.620 m, rise of 0.225 m, thickness 0.024 m). To the best of the authors' knowledge, no investigations on groin pointed vaults of the size at hand (2m x 2m in plan) have been carried out in the past.
The main objectives of the SEBESMOVA3D project were to assess the dynamic behaviour and evaluate the crack patterns and collapse mechanisms of groin vaults with different base boundary conditions, namely Configuration 1 in which the vault model rests on four fixed supports, and Configuration 2 where the vault model rests on two fixed springings combined with two one-directional moving supports characterised by very low lateral stiffness. The rationale behind this choice lies in the observation that a vault under earthquake excitation is mainly subjected to two distinct phenomena [19]: (i) dynamic response of the structure without relative support movements which can be modelled by Configuration 1, and (ii) response of the vault to differential horizontal ("in-plane shear") displacements imposed at its springings through the non-uniform response of underlying structures such as walls and piers, characterised by different lateral stiffness, which can be modelled by Configuration 2. Four different conditions were considered along the four lateral edges to account for different confinement levels: wooden panels, Plexiglas panels (cut and uncut) and no panels.

The aim of this paper is to: (1) outline the main features of the novel specimen design and the cutting-edge experimental setup (e.g. high definition motion capture equipment), and (2) elucidate the main findings of the experimental campaign with emphasis on the effect of different boundary conditions both at the base of the vault and laterally. The generic vault model employed in the study is representative of masonry and stone cross vault structures which are common in the Mediterranean region. A detailed interpretation/simulation of the test results and extrapolation to real vaults is beyond the scope of the present manuscript and will be the subject of a companion paper.

2 The vault model

To investigate the structural response of masonry groin pointed vaults, a scaled model was built to realistically simulate the geometry, mass distribution, and interface behaviour of this type of structures. As no specific prototype structure was targeted, a generic configuration based on typical proportions and a circular profile for the intersecting barrels were adopted. The diagonal intersections were also semi-circles for ease of construction, resulting in inclined vertices. It should be noted that considering ribs with the vault would have added further complexity both in construction and the dynamics of the model, so they were avoided in this study. The model was designed as an assembly of distinct plastic-mortar blocks. A plastic mould formed each block, made by a 3D printer at the Bitonto FabLab (Italy), which was then filled with mortar to acquire the necessary mass for dynamic tests. Gum layers were laid at the interfaces to control the adequate friction between the blocks. The shape and dimensions of the blocks were carefully designed through stereotomy studies of real stone and masonry vaults [35], [36]. In this way, every block was designed to play an essential part in the stability and static equilibrium of the vault.

Studying damage of historic buildings in seismic events reveals that failure of vaults does not initiate at their springings, but at the key-stone zone which is essentially embedded into support elements to counteract the outward thrust [37], [38], [39]. Examples are displayed in Figure 1. This is a key element to be considered when attempting to understand and predict the response of masonry vaults to seismic action. For this reason, the model was truncated at the base to take into account the effect of embedment in the perimeter walls and stiff springings (Figure 2).

The global dimensions of the vault were adjusted to fit the capacity of table at EQUALS laboratory at the University of Bristol, leading to a physical model occupying a 2m x 2m area and standing at a height of 0.71m. (This model may correspond roughly to a scaling factor of 5 relative to a hypothetical 10 m x 10 m prototype with a rise of 3.5 m. Nevertheless, other scaling factors are possible [46]). The vault consists of 172 blocks, five of which have larger dimensions than the others. These are the four bases on which the structure is set up, Figure 3a, and the keystone, Figure 3b, which locks all the pieces into position. The average dimensions of a typical block are 12 cm x 8 cm x 20 cm, Figure 3c.

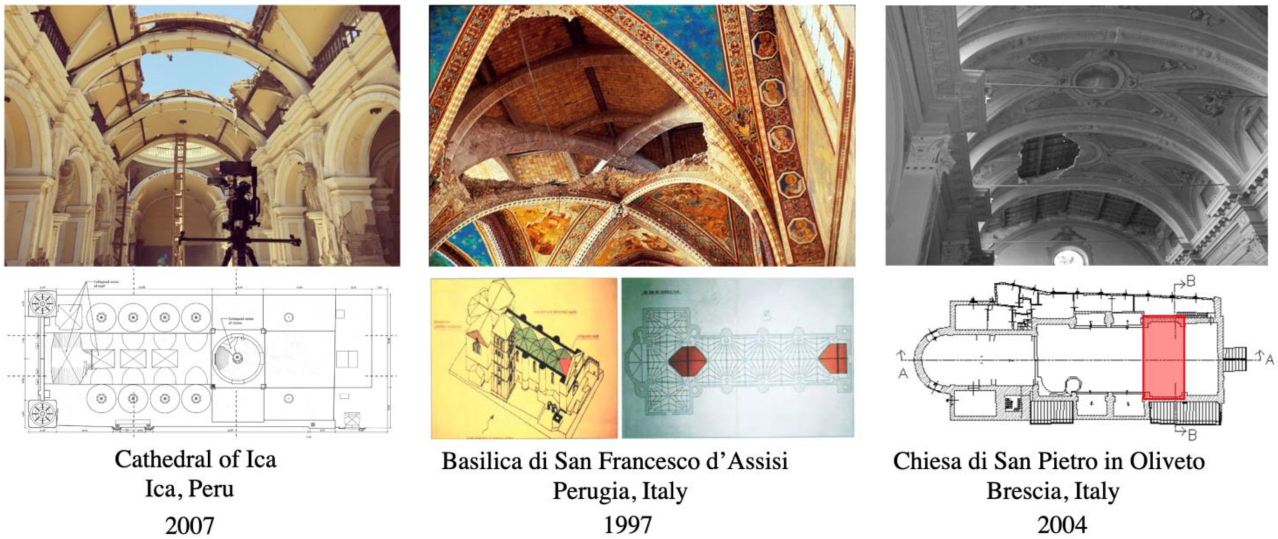

Figure 1: *Examples of vault collapses in historical churches [37], [38], [39].*

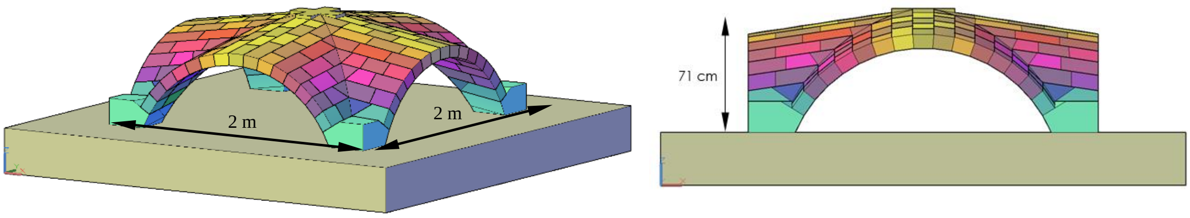

Figure 2: *The vault model.*

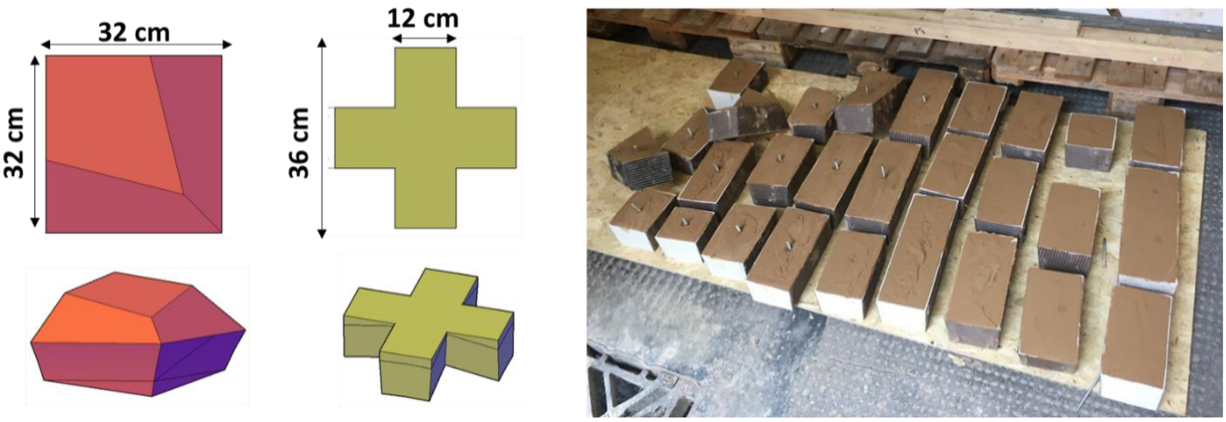

(a) *(b)* *(c)*

Figure 3: *(a) Base block. (b) Keystone block. (c) Typical blocks.*

3 Material properties

The composite blocks of the vault are fastened to each other with a thin layer of gum to increase the frictional and dissipative properties of the interfaces, and allow for small adjustments to be made during construction, since no fresh mortar exists between the bricks. The internal friction angle of the gum-enhanced interface between adjacent blocks was experimentally evaluated at about 30°.

The 3D printed blocks were made of polylactic acid (PLA) which is a completely compostable and biodegradable polymer obtained from the processing of plants rich in dextrose. The printing resolution in terms of layer height was 0.3 mm. The blocks are hollow with a thickness of plastic casing of about 2.5 to 3 mm.

The filling material of the blocks is "thistle bonding coat" made of British Gypsum. Mass density of the infill mortar was around 1.2 Mg/m^3. To assess the mechanical properties of the filling material, a compression test of a cubic sample was carried out, as shown in Figure 4. The elastic modulus (E) and compressive strength were estimated at 60 MPa and 250 kPa, respectively (a ratio of 240). Likewise, the mechanical properties of the mortar-skin-gum set were assessed via cyclic compressive tests of a chain of three bricks filled with mortar and a gum-layer around, Figure 5. The initial part of the first cycle of loading provides information about the elastic modulus of the gum (E = 0.8 – 1 MPa), as this is the first element of the mortar-skin-gum set that gets compressed. The subsequent part of the first loading cycle returns an elastic modulus of 40 MPa for the three bricks, which is mostly provided by the stiffness of the plastic box. At higher forces, mortar starts to engage as it is confined by the plastic box (E = 200 MPa).

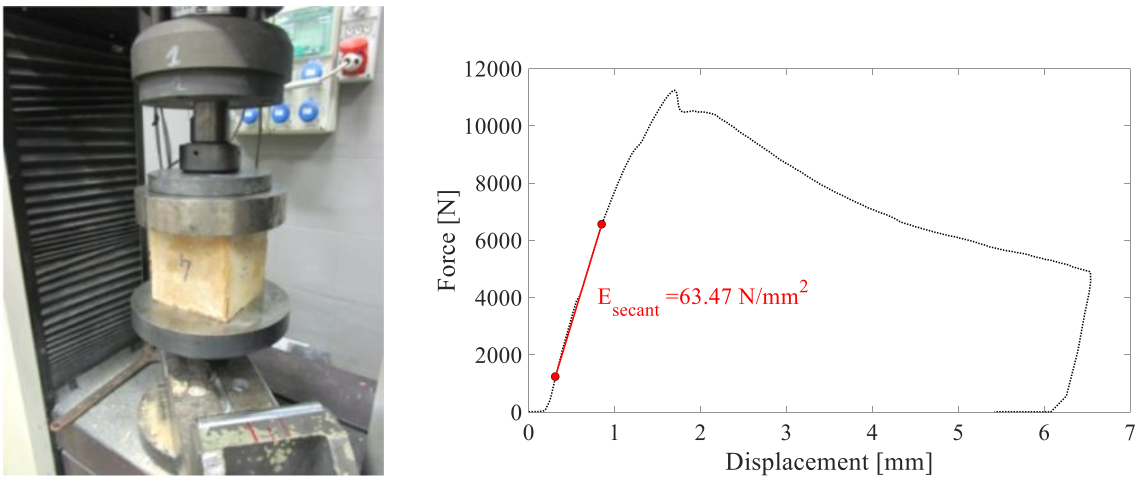

(a) *(b)*

***Figure 4**: (a) Setup of the compression test of a mortar cubic sample. (b) Force-displacement diagram.*

(a)

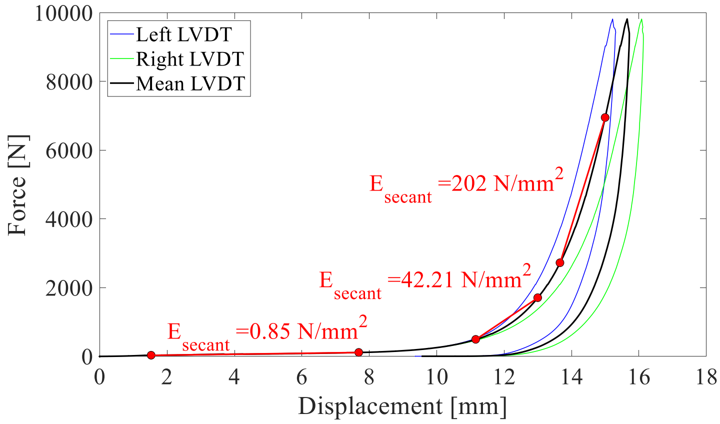

(b)

***Figure 5**: Cyclic compression tests of a chain of three bricks filled with mortar and bonded with a gum-layer: (a) setup of the tests, (b) elastic modulus of the gum layer, the plastic skin, the block (plastic skin and mortar).*

4 Construction phases

The plastic brick moulds were pre-assembled to verify dimensions, shapes and number of units, as shown in Figure 6. The vault was then dismounted to fill up the units with mortar. The vault was placed on four 2-cm thick steel corner plates designed to counteract the thrust at the springings and set the desired base boundary conditions. This is discussed in the following section.

The assembly process for each configuration was kept the same in the interest of repeatability of construction. The base blocks were first positioned on the steel plates, followed by blocks placed on the polystyrene formwork starting from the lateral arches. After each row of blocks was installed for all lateral arches, the diagonal blocks were installed followed by the remaining block of webs (Figure 7).

The total weight of the groin vault model filled with mortar was about 4.69 kN. The weight of each steel corner plate was around 0.9 kN, leading to an overall model weight of 8.3 kN.

Figure 6: *Pre-assembly of the plastic skin of the blocks.*

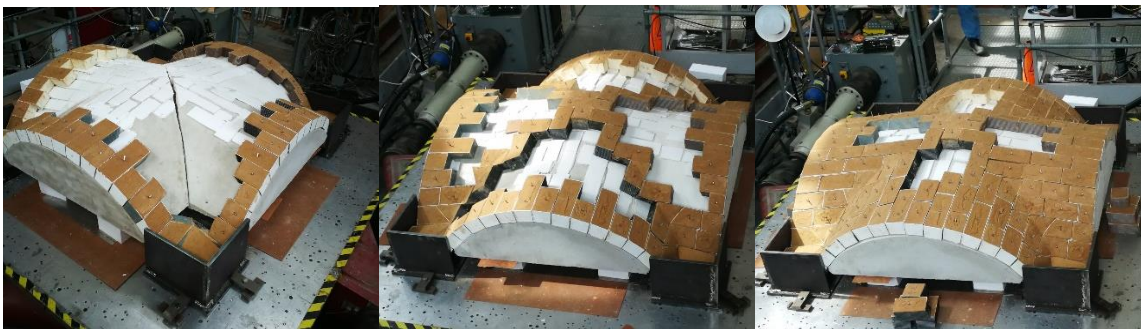

Figure 7: *Assembly process.*

5 Testing configurations

Various configurations were tested depending on two different base boundary conditions and four types of lateral confinement (Figure 8).

The two base boundary conditions considered are:

1. Fixed: the vault was placed on four steel plates fixed on the shaking table (Figure 8a).
2. Moveable: the vault was placed on two fixed steel plates and on two moveable carriages on bearings running in the Y direction along a pair of 40mm-diameter rails regulated by horizontal springs to provide a combined stiffness of 16 kN/m (Figure 8b).

The stiffness of the horizontal springs was designed to obtain an "in-plane shear" displacement roughly equal to 3% of the longitudinal arch span [19] (i.e. 60 mm) under a Peak Table Acceleration (PTA) of around 0.25 g, considering no amplification and half mass of the vault effectively acting on the springs. As discussed earlier, the configurations of fixed based and moveable springings will be referred in the following to as Configurations 1 and 2, respectively.

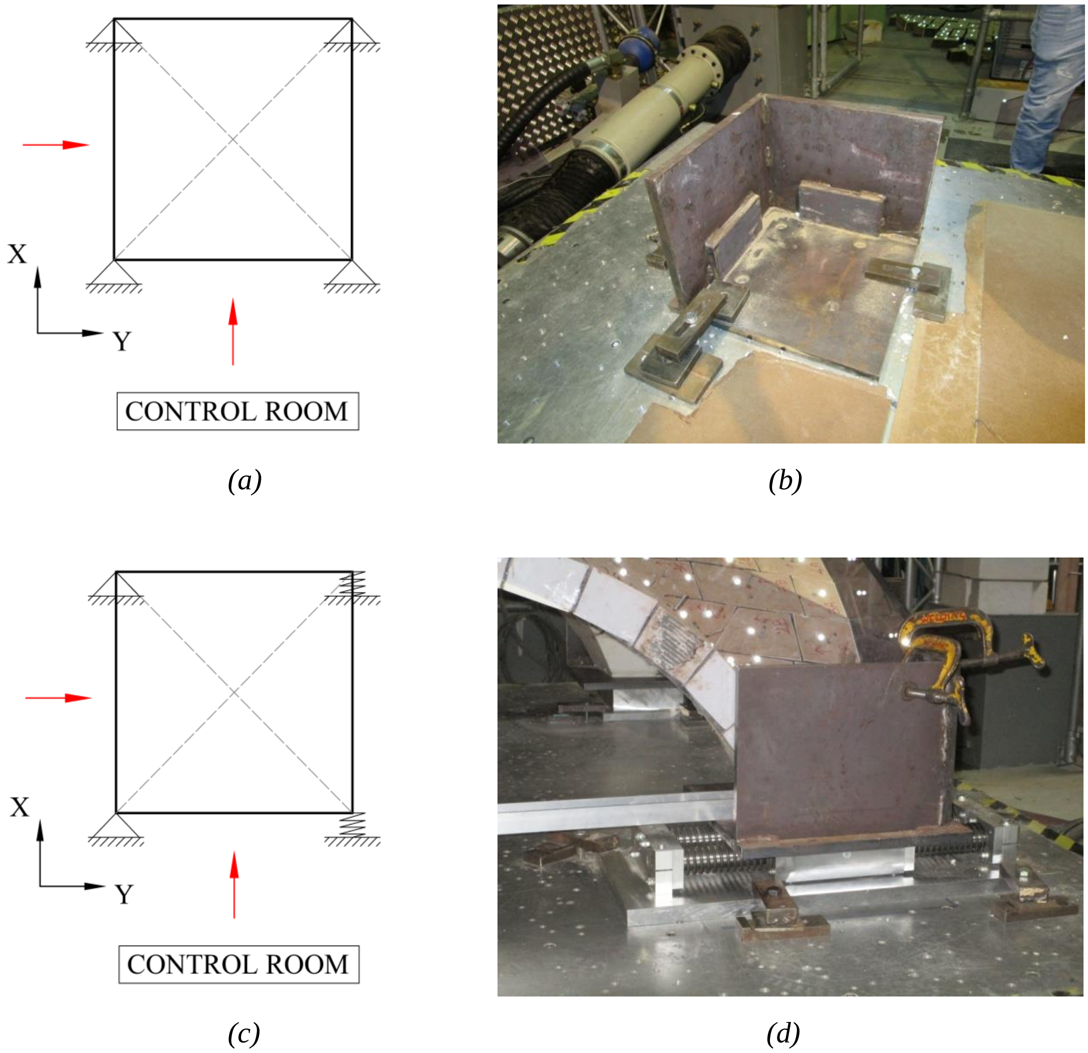

Figure 8*: (a) Scheme of Configuration 1: fixed. (b) Steel plates firmly clamped to the table to realise the fixed restraints. (c) Scheme of Configuration 2: moveable. (d) Steel plates mounted on a moveable carriage running on bearings controlled by horizontal springs to realise two flexible springings.*

Different lateral confinement types were provided along the lateral arches. Specifically:

A. Four 2 cm-thick wooden panels (elastic modulus about 7 GPa, Figure 9a).
B. Four 2 cm-thick Plexiglas panels (elastic modulus about 3 GPa, Figure 9b).
C. Four 2 cm-thick Plexiglas panels, with two of them (the ones along the Y-direction, normal to the direction of movement allowed by the carriages) cut in the middle (Figure 9c).
D. No panels but only spandrel confinement (Figure 9d).

Table 1 summarises the configurations tested, the nomenclature used to refer to each of these and the identification number of the corresponding tests.

(a) *(b)*

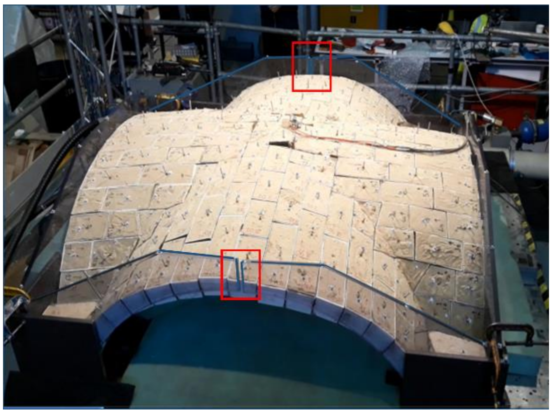

(c) *(d)*

Figure 9: *Different lateral confinements along the lateral arches: (a) four 2 cm-thick wooden panels, (b) four 2cm-thick Plexiglas panels, (c) four 2cm-thick Plexiglas panels, with two of them cut at the crown, (d) no panels.*

Table 1: *The configurations that were tested.*

Configurations	Base boundary condition	Lateral Confinement	Tests carried out
1A	1: fixed	A: Wooden panels	1-72
1B	1: fixed	B: Plexiglas panels	73-145,147, 176, 196, 200
1C	1: fixed	C: Cut Plexiglas panels	205,207, 209,211,213
1D	1: fixed	D: No panels	237,239,241,243,245,247,249,251,253,255,257, 259
2A	2: moveable	A: Wooden panels	Not tested
2B	2: moveable	B: Plexiglas panels	146, 148-175, 177-195, 197-199, 201-203
2C	2: moveable	C: Cut Plexiglas panels	204, 206,208,210,212, 214-236
2D	2: moveable	D: No panels	238,240,242,244, 246, 248,250, 252, 254, 256,258, 260-266

6 Testing instrumentation

The nomenclature of the webs and ribs is reported in Figure 10a. The testing instrumentation consists of: (a) two triaxial Setra accelerometers situated on the shaking table and the keystone of the vault, sampling at a rate of 5000 Hz (Figure 10b); (b) a vision system consisting of motion-capture cameras recording the positions at a rate of 100 Hz, of reflective markers positioned on each block for individual block tracking, on the panels and on the shaking table (Figure 10c); (c) a data acquisition system encompassing a 250-channel system and an advanced wireless system of 8 high-definition digital cameras.

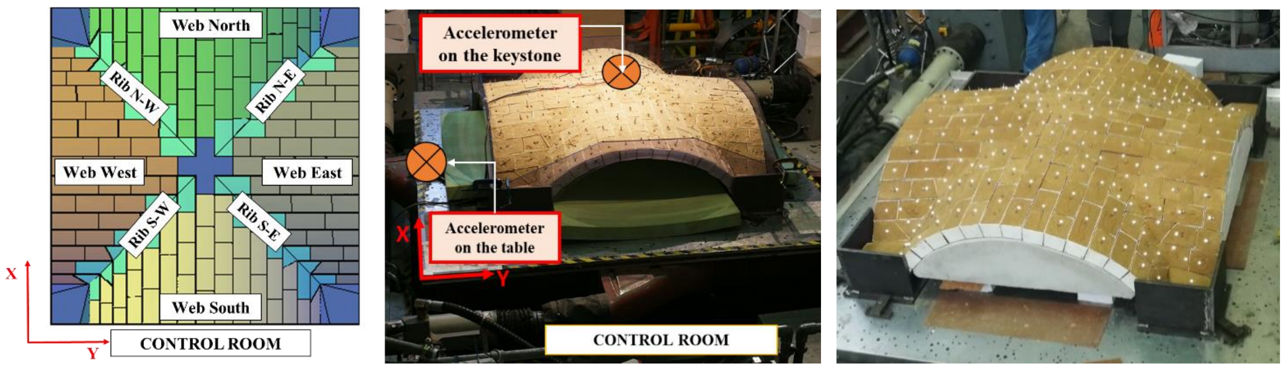

(a) (b) (c)

***Figure 10**: (a) Reference system. (b) Position of the triaxial Setra accelerometers. (c) Position of the reflective markers.*

7 Testing programme

During the experimental campaign, 266 tests were carried out on two separate sessions, August 2019 and January/February 2020. The whole set of tests is listed on Table A1 in the Appendix. Considering that the restraining (stabilising) action is associated with self-weight and the driving (destabilising) action is associated with inertia, Housner's rocking model [40] suggests that the time scale should be equal to the square root of the geometric scaling factor, i.e. $\lambda_{time} = (\lambda_{geometry})^{1/2}$. For a geometric scaling factor of approximately 5 to 10 (in agreement with scaling factors available in the literature for models of similar size [46]), this implies that dynamic time is scaled by a factor of roughly 2 to 3. It should be kept in mind, however, that the modelling is distorted relative to a real vault, since stress similitude is not preserved (e.g. the elastic moduli of the materials are not faithfully scaled). This violation, however, is of minor importance for the purposes of the experiments at hand, as the sliding/rocking behaviour of the structure prevails near failure and is not affected by elastic behaviour [41].

In the first session, tests 1 to 63 were conducted in three stages: each of them was realised in a series of consecutive tests with reconstruction only after collapse, meaning that each test accumulated the damage (block dislocations) of the preceding ones. In this session, the vault was resting on four fixed supports with four 2 cm-thick wooden panels mounted along the lateral arches (Configuration 1A). Sinusoidal tests of constant excitation amplitude with varying frequencies between 1 Hz and 50 Hz were performed, with special emphasis in the frequency range 2 – 15 Hz, where the effects of resonance were significant and most of the damage took place. Additionally, six seismic tests were performed by applying real recorded motions from the Emilia 2012 earthquake (Modena and Mirandola stations) and El Centro 1940 NS. At the beginning of each stage, white noise tests with an approximate Root Mean Square (RMS) table acceleration of 0.05 g, were applied to obtain the dynamic properties of physical model. This was important to ensure that the model was rebuilt with the same configuration, exhibiting more or less the same frequency response, leading to repeatable tests. During this session, the vault collapsed three times: two at an excitation of 2 Hz with a Peak Table Acceleration (PTA) of 1 g (tests #31 and #52), and one at 5 Hz with a PTA of 1.4 g (test #63).
In the second session, all configurations were tested through a series of random tests of gradually increasing acceleration:

- RMS acceleration range 0.02 g – 0.60 g for Configuration 1A (tests #64 to #72);
- RMS acceleration range 0.03 g – 0.22 g for Configuration 1B (tests #73 to #78);
- RMS acceleration range 0.04 g – 0.20 g for Configuration 2B (tests #146 and #148 to #151), for Configurations 1C and 2C (tests #204 to #213) and for Configurations 1D and 2D (tests #237 to #244).

To this end, suites of sinusoidal tests involving 10 excitation cycles of constant amplitude and decreasing frequency (from 50 Hz to 1 Hz), were carried out on Configurations 1B, 2B and 2C, in a similar fashion to the first session. Moreover, for Configurations 1B, 2B, 1D and 2D, sinusoidal tests were performed focusing on low-frequencies (1–2–3–5 Hz). In general, collapse was reached, via damage accumulation, after a considerable number of successive tests. An exception was tests #142 and #143 in which the collapse input motion of the preceding test was applied right upon reconstruction of the model, to investigate the importance of damage accumulation.
Long sinusoidal input (500 cycles) of constant amplitudes (0.2 g – 0.3 g) and low frequencies (3–2.5–2 Hz) were applied during tests #197-198 and #201-203, to investigate possible low-cycle fatigue phenomena. It was observed that 1000 cycles at 3 Hz, as well as 1000 cycles at 2.5 Hz were not sufficient to induce full collapse. Collapse occurred when the input frequency was lowered again

to 2 Hz, highlighting the strong dependence of collapse on excitation frequency than duration, for lower acceleration levels (around 0.2 g).

For Configuration 1B, three collapses were recorded: one at 5 Hz with PTA = 0.75 g (test #118) and two at 3 Hz with PTA = 1 g (test #139 and #143). Also, in Configuration 2B, the vault collapsed three times: at 2 Hz with PTA = 0.25 g (test #174) and 0.2 g (test #203) and at 3 Hz with PTA = 1 g (test #194, partial collapses started at 0.5 g). For Configurations 2C and 2D, only one collapse was recorded: at 2 Hz with PTA = 0.25 g (test #236) and at 3 Hz with PTA = 0.4 g (test #266), respectively.

8 Results of white noise tests: dynamic properties

White noise tests were systematically carried out in each model configuration for dynamic identification purposes, including amplitude dependent effects. Noiseless frequency response functions were obtained from the white-noise response data using the curve-fitting algorithm of an Advantest R9211B FFT servo analyser configured to compute the poles and zeros of the complex functions in the Laplace domain. Damping coefficients and resonant frequencies at the peaks of the fitted frequency response function waveforms were then obtained from the real and imaginary parts of the computed poles.

As already mentioned, the vault was tested repeatedly up to collapse and then rebuilt; after each reconstruction, low-amplitude (0.03 – 0.05 g) white noise tests were conducted to check whether the model was rebuilt to the same configuration and possessed the same dynamic properties. For a given configuration, they highlighted the substantial equivalence/repeatability of the tests in terms of fundamental frequency and damping ratio, of each reconstruction with respect to the preceding one.

Figure 11 displays the fundamental frequency of the vault as a function of the RMS table acceleration for all the investigated configurations. In all cases, the plots suggest that the fundamental frequency is amplitude-dependent, indicating a decrease with increasing acceleration. Also, as expected due to a reduction in stiffness, Configuration 2 (two moveable springs) is characterised by significantly reduced frequencies. Finally, the vaults without panels are more flexible, providing frequency values roughly equal to half of those of the corresponding confined vaults. This strong non-linear dynamic behaviour of the model could be explained in light of detachments between the bricks in many places during high amplitude shaking, leading to an "equivalent/effective" Young's modulus of the vault which continuously changed in time and space.

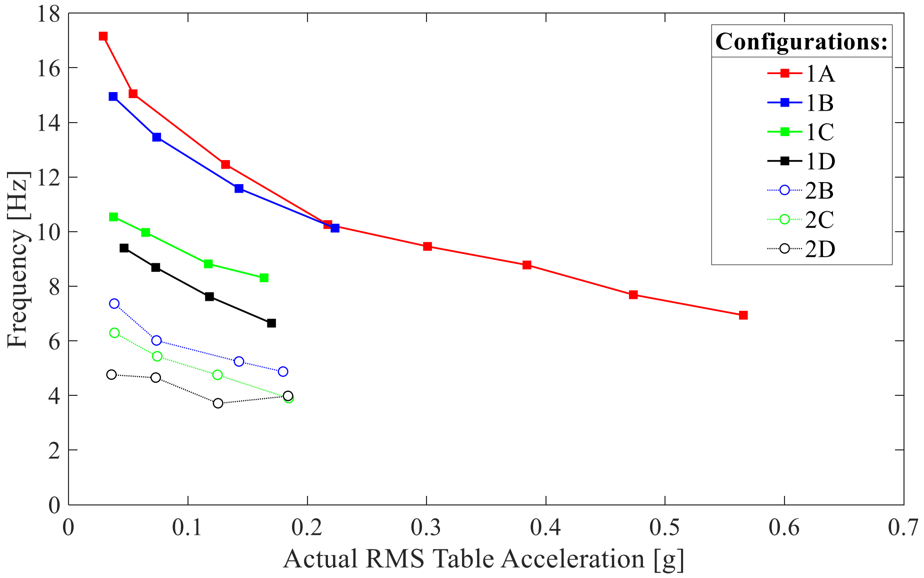

Figure 11*: Fundamental frequency as a function of acceleration for all investigated configurations.*

Regarding the Percentage of Fixed Connection (*PFC*) provided by the flexible supports, according to elementary mechanics & soil-structure interaction theory [47], the combined stiffness of two translational linear springs k_s (representing the stiffness of the structure) and k_b (representing the stiffness of the base spring) attached in a series is $k = k_s\, k_b\, /(k_s + k_b)$. The corresponding natural frequency is $f = (k/m)^{1/2}$, m being the engaged inertial mass. Considering the natural frequency of the structure on fixed supports $f_s = (k_s/m)^{1/2}$ and assuming that the inertial mass is the same between the two configurations, yields $(f\,/f_s)^2 = 1/(1 + k_s/k_b)$. Evidently, if k_b gets infinitely large, the frequency ratio $(f\,/f_s)$ on the left hand side will tend to 1. This condition will be called 100% of a fixed connection. Conversely, if k_b tends to zero, the frequency ratio $(f\,/f_s)$ will tend to zero as well, which will be called 0% of a fixed connection. Accordingly, *PFC* can be determined from the expression:

$$PFC = \left(f / f_s \right)^n \cdot 100 \ (\%) \qquad (1)$$

where $(f\,/f_s)$ stands for the experimentally measured ratio of natural frequencies of the vault with and without movable supports, recorded at the same excitation intensity, and n is a pertinent power (taken here equal to 2 following the above analytical developments). Application of this equation yield values on the order of 30%, as reported in Table 2.

Table 2: *Percentage of Fixed Connection (PFC).*

Configuration	**Test N.**	**PTA** [g]	***f$_s$*** [Hz]	**Test N.**	**PTA** [g]	***f*** [Hz]	**PFC** [%]
B	147	0.03	13.29	151	0.04	6.88	26.80
	176	0.03	13.86	180	0.04	6.87	24.57
	196	0.04	12.65	195	0.04	7.24	32.76
	200	0.04	13.71	199	0.04	6.97	25.85
C	205	0.04	10.54	204	0.04	6.29	35.61
	207	0.06	9.97	206	0.07	5.4	29.34
	209	0.12	8.82	208	0.12	4.75	29.00
	211	0.16	8.31	210	0.18	3.9	22.03
	213	0.04	10.78	212	0.04	6.47	36.02
D	237	0.05	9.4	238	0.04	4.76	25.64
	239	0.07	8.69	240	0.07	4.65	28.63
	241	0.12	7.62	242	0.13	3.71	23.70
	243	0.17	6.65	244	0.18	3.98	35.82
	251	0.04	10.12	252	0.04	5.57	30.29
	255	0.04	10.16	256	0.04	5.41	28.35
	259	0.04	9.78	260	0.04	5.66	33.49

Figure 12 illustrates the relationship between the back-calculated values of damping ratio and input RMS table acceleration for all the investigated configurations. Firstly, relatively high values of damping (around 10% or larger) were obtained, due to the considerable dissipative properties of the gum layer. Secondly, the damping ratio increases with table acceleration, due to the large movements and/or detachments of the blocks. As expected, Configuration 2 provides larger values relative to Configuration 1, for which the effect of the confinement panels seems to be more significant, especially at low acceleration levels (0.05g). Similarly to Figure 11, the damping ratio is seen, on average, to be amplitude-dependent indicating a general increasing trend for Configuration 1.

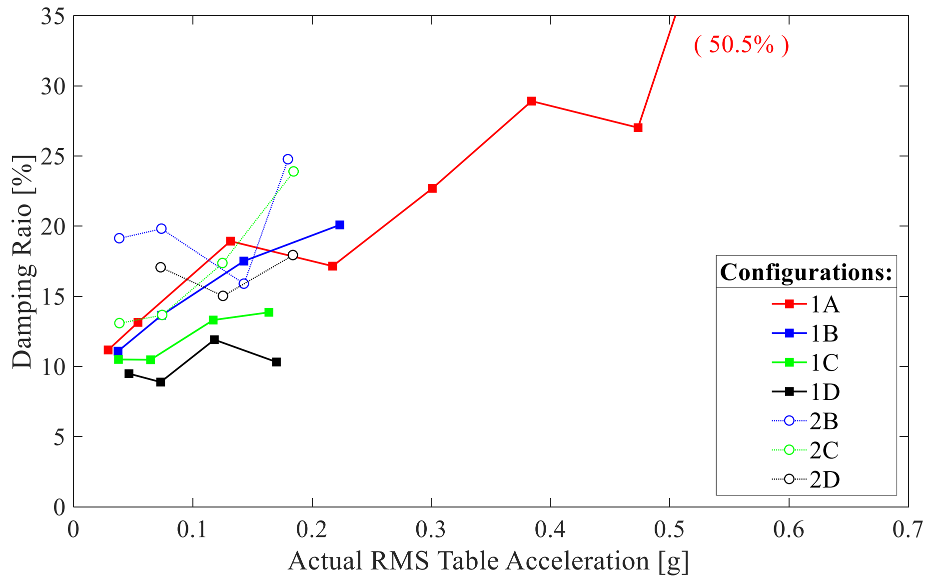

***Figure 12**: Damping ratio as a function of acceleration for all the investigated configurations.*

Figure 13 displays the amplification factor obtained from the ratio between the RMS acceleration recorded by the accelerometers on the keystone and on the table. The amplification factor decreases with increasing acceleration, which, in turn, strongly relates to the corresponding increase in damping ratio. The amplification factors can be grouped together for Configurations 1A and 1B (continuous panels) and Configurations 1C and 1D (interrupted or no panels) and follow the same trend. The difference between these groups highlights the effect of lateral confinement: the stronger the confinement, the larger the amplification factor. The absence of a continuous lateral confinement for the arches parallel to the input direction (i.e. absence or interruption of panels orthogonal to the input direction) leads to far smaller - by more than 3 times - amplification factors. As far as Configurations 2 are concerned, the presence of moveable springings forces the amplification factors into a single band, comparable with those obtained for Configurations 1A and 1B.

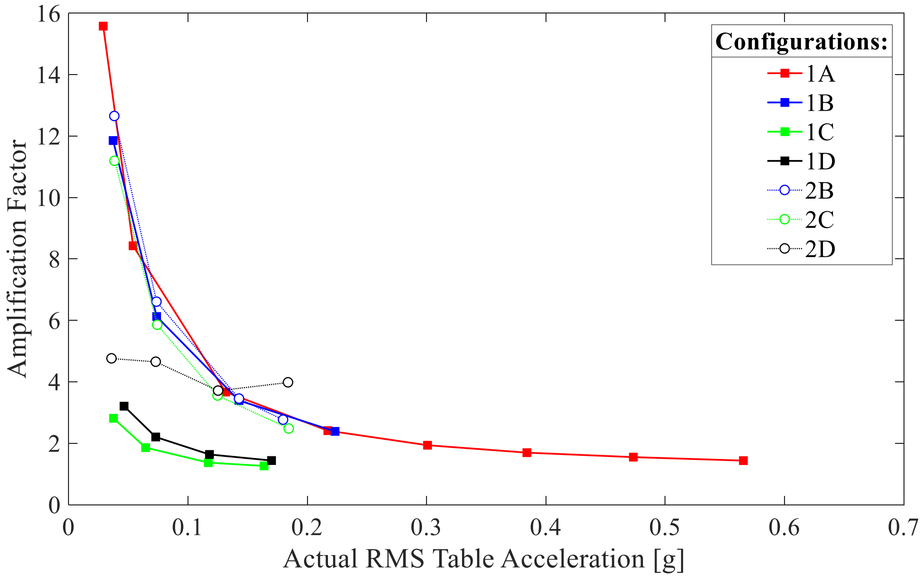

Figure 13: *Amplification factor (ratio of RMS accelerations) as a function of acceleration for all the investigated configurations.*

9 Preliminary observations from sinusoidal tests

Simple inspection of Table A1 allows the following observation to be made: all other conditions being the same (i.e. same lateral confinement given by the Plexiglas panels) and under low-frequency excitation, Configuration 2 (subjected to differential horizontal "in-plane shear" displacements at the supports through two moveable springs) reaches collapse at a lower acceleration than Configuration 1 (subjected to uniform motion at four fixed supports). Specifically, Configuration 2 collapsed for an acceleration of around 0.4 g (i.e. average between total collapse at 0.25 g for 2 Hz input and partial collapse at 0.5 g for 3 Hz input), whilst Configuration 1 collapsed at around 1 g for a 2 Hz input. This suggests that the pseudo-static response of the vault induced by imposed "in-plane shear" displacements at its springings often represents the predominant cause of damage/failure, overshadowing the dynamic response of the vault itself [19].

The analyses of the cumulative displacements within the different series of tests and the collapse accelerations obtained in test #139 (collapse after cumulative damage due to several successive sinusoidal excitations) and test #143 (direct application of the collapse excitation imposed on the preceding test) show that the specific vault is not particularly susceptible to cumulative damage.

The time-histories of displacements obtained by the vision data system for the marker on the keystone were analysed in order to: (i) obtain the maximum displacement recorded during each test and (ii) evaluate the cumulative displacements before collapse within the test sequences.

Figures 14, 15 and 16 illustrate the peak recorded relative (with respect to the shaking table) horizontal displacement of the keystone during the sinusoidal series of tests for Configurations 1A, 1B, 2B and 2C, respectively. It can be seen that for all the tested configurations, the physical model was vulnerable to low frequencies, especially near 2 Hz, whose maximum induced displacements far exceeded those produced at higher frequencies and same accelerations. Keystone maximum relative horizontal displacements to high-frequency inputs such as 50 Hz, 20 Hz or 15 Hz exhibited an almost horizontal asymptotic trend with increasing acceleration, without exceeding values around 0.5 mm. Inputs of 2 Hz induced considerable movements (unexpected amplification), which may indicate that the “effective” fundamental frequency of the nonlinear physical model is around that value, at least for large acceleration amplitudes (> 0.6 g for fixed boundary conditions and > 0.25 g for moveable ones), for which it was not possible to perform random motion tests. As expected, the vault model in Configuration 2 is more flexible. Indeed, the keystone max relative displacements recorded for Configuration 2 (Figures 15b and 16) are around 10 times higher than those recorded for Configuration 1 at the same acceleration level (Figures 14 and 15a).

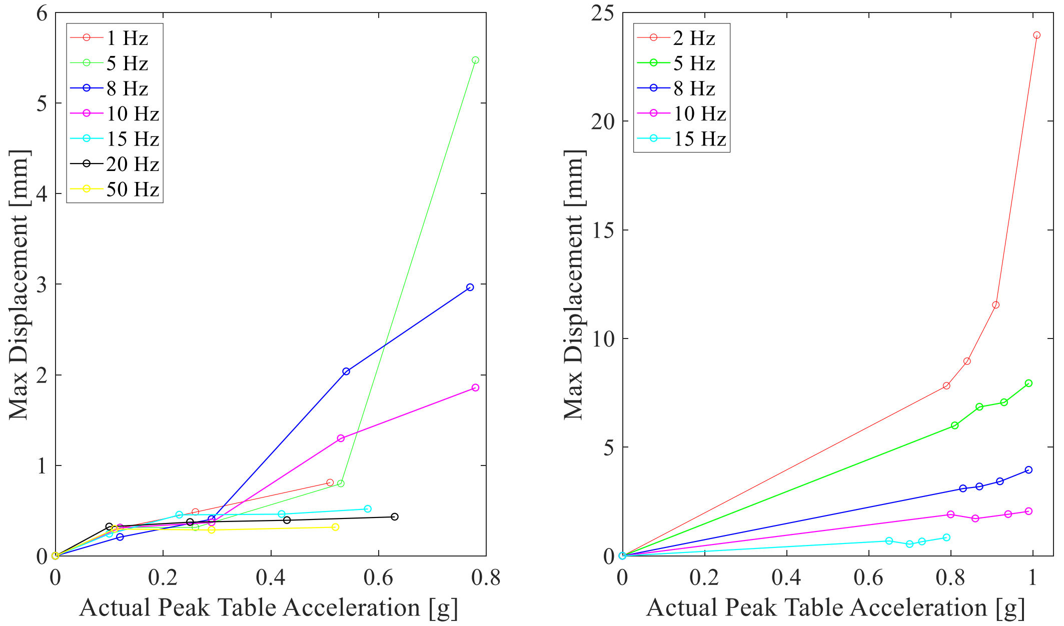

(a) *(b)*

Figure 14: *Maximum relative horizontal displacement of the keystone as function of the PTA for sinusoidal input characterised by different frequencies and Configuration 1A: (a) series of tests #4 to #30 and (b) series of tests #33 to #52. Note the large difference in scale of displacement.*

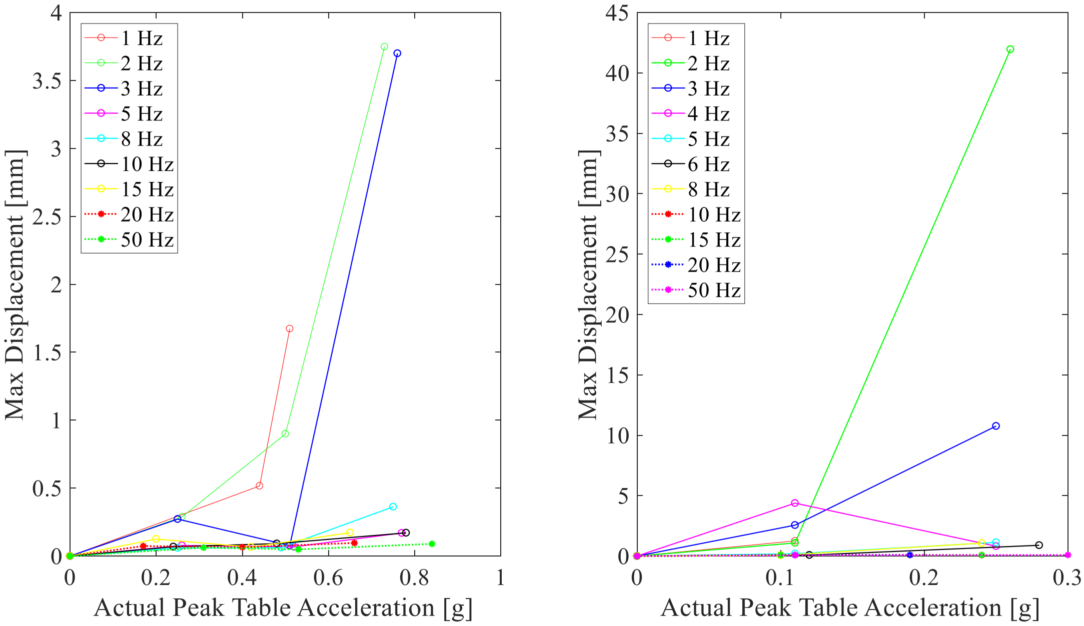

(a) *(b)*

Figure 15: *Maximum relative horizontal displacement of the keystone as function of the PTA for sinusoidal input characterised by different frequencies: (a) series of tests #79 to #106 for Configuration 1B and (b) series of tests #152 to #173 for Configuration 2B. Note the large difference in scale of displacement.*

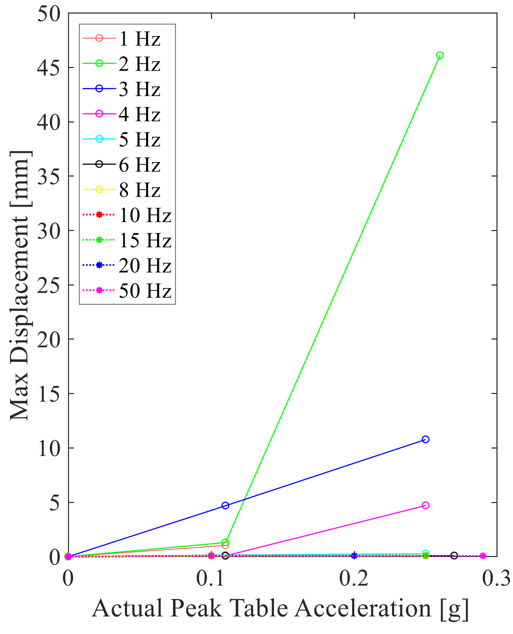

Figure 16: *Maximum relative horizontal displacement of the keystone as function of the PTA for sinusoidal input characterised by different frequencies for Configuration 2C: series of tests #214 to #235.*

Since no reassembly of blocks was done prior to collapse, each test naturally starts from a displaced condition that can be interpreted as an accumulated damage state. Figures 17-20 report the residual displacements at the end of each sinusoidal test that accrue along the test series until collapse is reached. The sequences investigated involve sinusoidal tests with duration of 10 cycles and frequencies in the range of 1 – 50 Hz for each step of increasing acceleration levels.

Figure 17 shows the cumulative residual displacements of the keystone for the test sequences before collapse at a PTA of 1 g for Configuration 1A. A jump in residual displacements is observed each increase of acceleration, while no significant residual displacements are provoked by a change of frequency. In the horizontal direction parallel to the applied input (X), the cumulative displacement before the last test of the first sequence is around 1.5 mm, while in the vertical direction (Z) it is 13.5 mm.

Figures 18a and b show the cumulative residual displacements for Configuration 1B, as obtained under a 10-cycle harmonic tests sequence and 100-cycle harmonic tests sequence, respectively. On one hand, the collapse at a PTA of 0.75 g was not achieved after 3 series of 10-cycle sinusoidal tests, reaching a final residual displacement of around 0.18 mm (after a peak value of around 0.25 mm) in the horizontal direction and 3 mm in the vertical direction (Figure 18a). On the other hand, the collapse at a PTA of 0.75 g was achieved after eight low-frequency (3 – 5 Hz) 100-cycle sinusoidal tests (Figure 18b). The final residual displacement reached before collapse was induced by the long input was larger than the one measured for the short input: around 3.3 mm in the direction of excitation (X) and 70 mm in the vertical one (Z).

The order of magnitude of residual displacements recorded before collapse at a PTA of 0.25 g for Configurations 2B (Figure 19) and 2C (Figure 20) are the same: 1 – 2 mm in the horizontal direction and 10 – 13 mm in the vertical one. In this case of moveable springings, there is a sudden dramatic effect with decreasing input frequency, specifically from 4 Hz to 3 Hz (partial collapses at double residual displacements) and finally at 2 Hz (total collapse).

In general, in the vertical direction and except for some rare cases in which small adjustments occurred, the displacements accumulate downwards, whilst in the horizontal direction displacements can pile up, sometimes towards one side and sometimes towards the other, thus providing a response pattern reminiscent of “structural resurrection” [42].

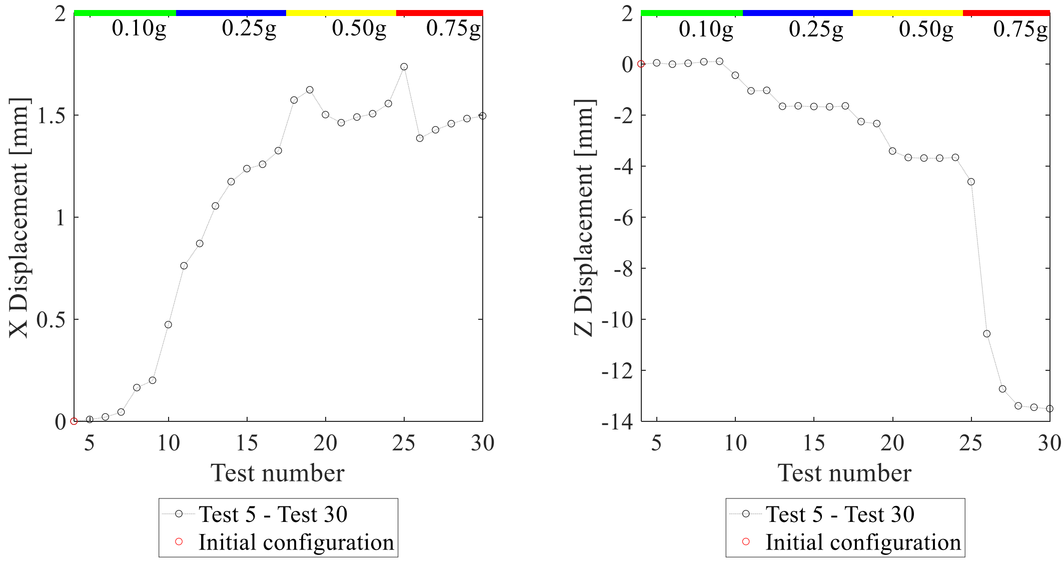

Figure 17: *Cumulative absolute residual displacement in X (horizontal) and cumulative residual displacement in Z (vertical) directions for Configuration 1A series of tests #5 to #30.*

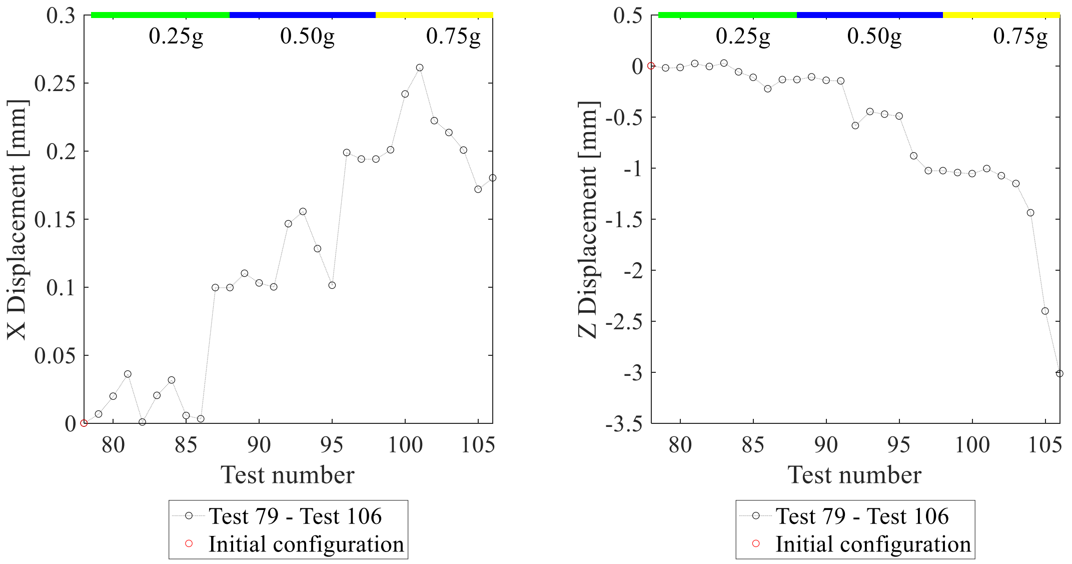

(a)

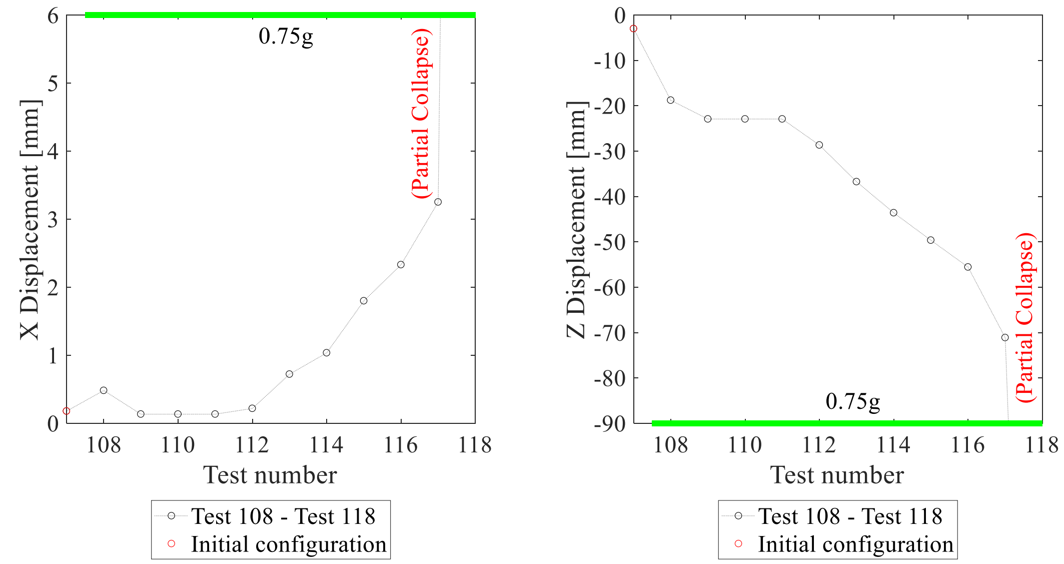

(b)

Figure 18*: Cumulative absolute residual displacement in X (horizontal) and cumulative residual displacement in Z (vertical) directions for Configuration 1B: (a) series of tests #79 to #106; (b) series of tests 108-109 and 112 to 118 input characterized by 100 cycles.*

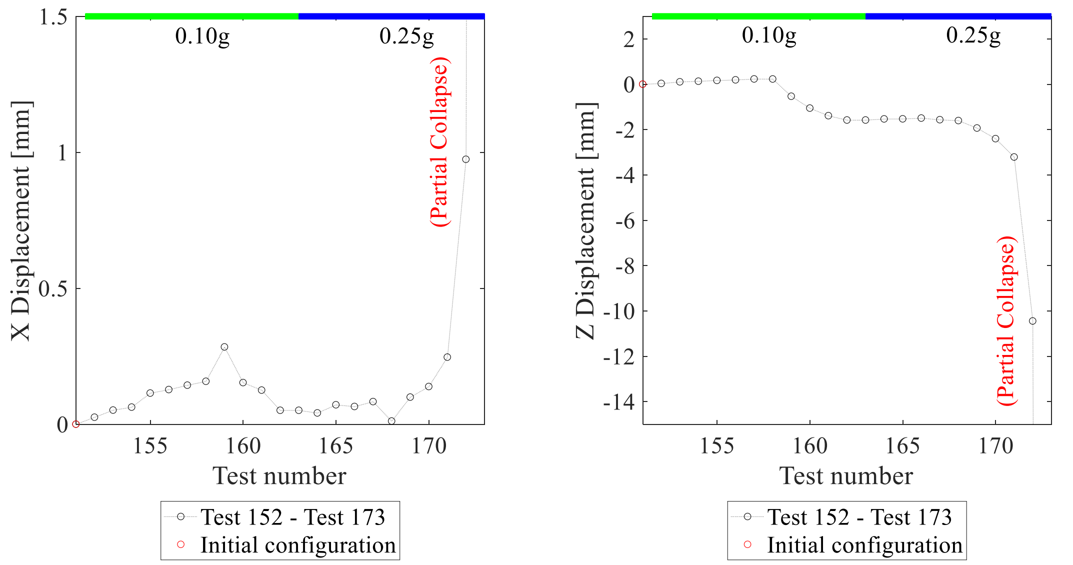

Figure 19*: Cumulative absolute residual displacement in X (horizontal) and cumulative residual displacement in Z (vertical) directions for Configuration 2B series of tests #152 to #173.*

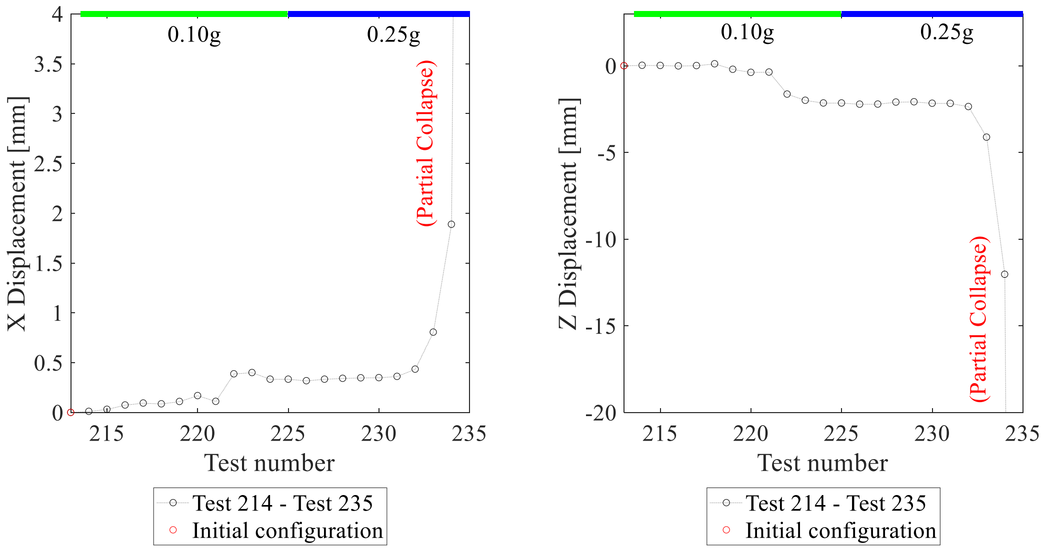

***Figure 20**: Cumulative absolute residual displacement in X (horizontal) and cumulative residual displacement in Z (vertical) directions for Configuration 2C series of tests #214 to #235.*

The failure mechanisms observed for the various experimental configurations can be characterised by two different collapse behaviours, which correspond to the two base boundary conditions employed: fixed and moveable.

For the fixed configuration, the deformed shapes recorded just before collapse appear symmetric and are characterised by a failure event, namely the formation of a cylindrical hinge on the upper central part of the vault, orthogonal to the input direction (marked with arrows in Figure 21).

In contrast, for the moveable configuration, the crack pattern shows a typical shear damage, and the failure starts with a diagonal crack at the North web until the progressive collapse of the central part and the West web (Figure 22). Mechanical failure was mostly the result of shearing causing dislocations and crack propagation. The crack pattern observed before collapse is similar to that obtained earlier by some of the authors with pseudo-static tests that investigated the effects of in-plane shear displacements at the springings of cross vaults [19], [43]. It is worth noticing that this crack pattern is in agreement with that detected at the intrados of the nave vaults next to the façade (same boundary conditions as in Configuration 2) in churches following major earthquakes [44], [45]. The different lateral confinement does not seem to significantly influence the failure mechanism.

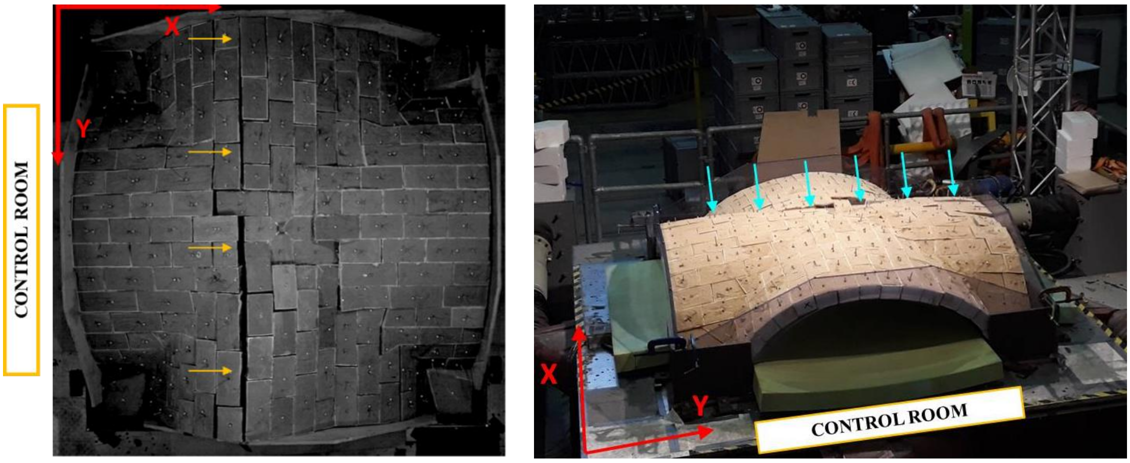

(a) (b)

Figure 21: *Failure mechanism at: (a) 2Hz with PTA 1 g for Configuration 1A, (b) 3Hz with PTA 1 g for Configuration 1B.*

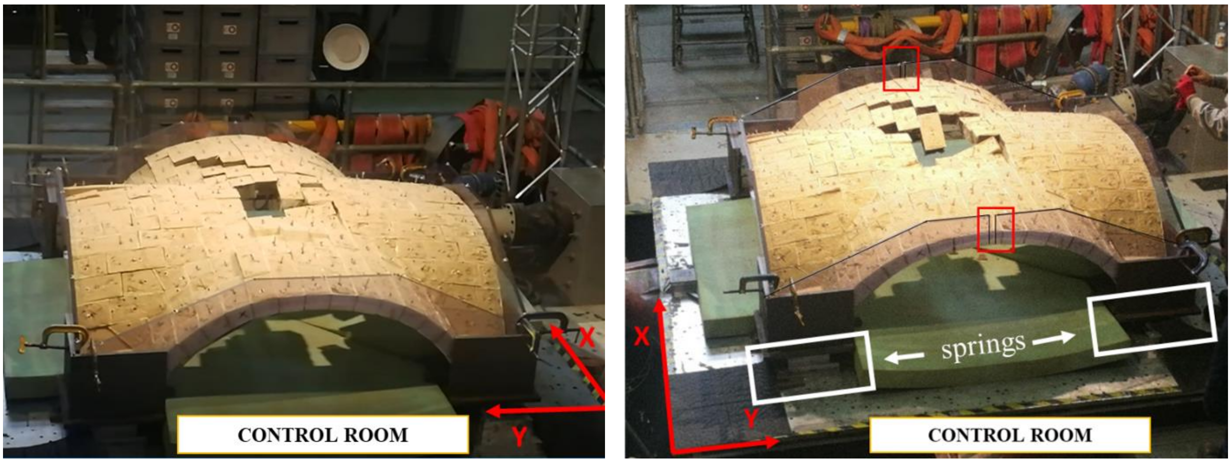

(a) (b)

Figure 22: *Failure mechanism at :(a) 2 Hz with PTA 0.25 g for Configuration 2B, (b) 2 Hz with PTA 0.25 g for Configuration 2C.*

10 Earthquake tests

Tests #56 to #60 were performed using three real acceleration records (Modena and Mirandola stations from the Emilia 2012 earthquake and El Centro 1940 NS). These tests did not induce any visible damage on the vault.

Figure 23 compares the acceleration time-histories recorded on the keystone for the three sinusoidal tests #25 - #26 - #30, with PTA's of around 0.7 g and frequencies of 2 Hz, 5 Hz and 20 Hz, respectively, and for the El Centro earthquake record with a PTA of around 0.7 g. These plots provide further confirmation as to the nonlinear response of the model, which is characterised by an "effective" fundamental frequency that decreases with increasing acceleration (Fig. 11). Specifically, for a PTA of around 0.7 g, extrapolation of the results reported in Fig. 11 (note it was impossible to apply random input motions with higher PTA) indicates that the effective fundamental frequency of the model in Configuration 1A is close to 6 Hz. Figure 23 shows that the fundamental frequency is closer to 5 Hz, since the keystone response to the 5 Hz harmonic input displays a larger amplification factor (around 2.6) with respect to those obtained for higher frequency input (test #30 with an amplification of slightly above 1) and a lower one (test #25, no amplification). Figure 24 displays the pseudo-acceleration spectrum of the signal recorded by the accelerometer on the table during test #58, which indicates that the predominant frequencies of the earthquake input are around 1.5 Hz, i.e. far from the 5-6 Hz range of the model at acceleration levels of 0.7 g. For this reason, the El Centro input was not as critical for the model as the other ones, since it would require higher accelerations (on the order of 1 g) that were not applied, to induce damage.

Extrapolation of the results to real vaults, other than the general significance of the non-linear response identified for the models at hand, lies beyond the scope of this paper.

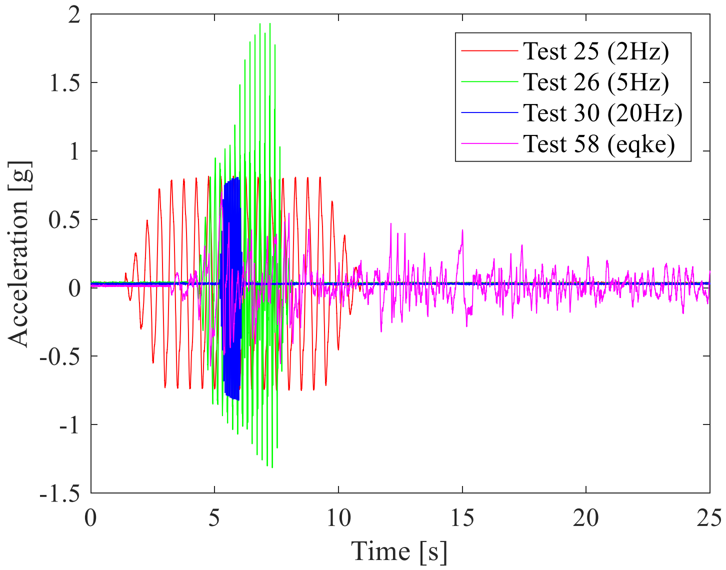

Figure 23: *Comparison between the acceleration time-histories recorded on the keystone during the sinusoidal tests #25 (PTA = 0.74 g, 2 Hz) - #26 (PTA = 0.78 g, 5 Hz) - #30 (PTA = 0.63 g, 20 Hz) - and the seismic test #58 (El Centro earthquake).*

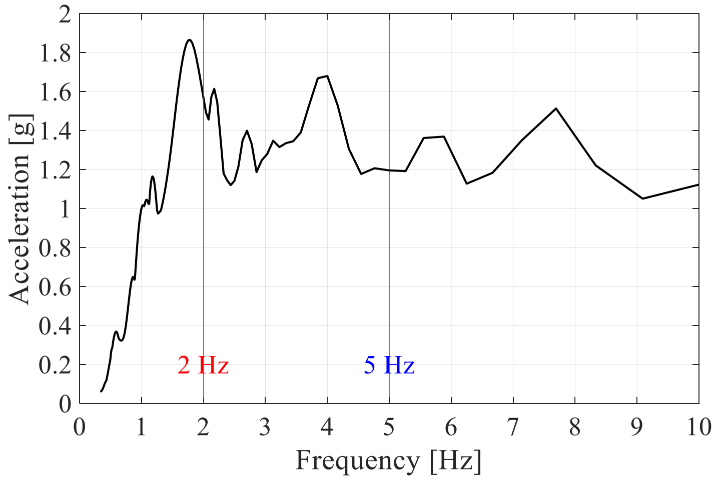

Figure 24: *Pseudo-acceleration spectrum (ξ=5%) of the signal recorded during test #58 (El Centro earthquake).*

11 Conclusions

A novel experimental campaign encompassing 266 shaking table tests was carried out at EQUALS laboratory, University of Bristol, UK, on a 2m x 2m x 0.7m scaled groin vault model made of plastic 3D printed blocks filled with mortar. The advantages of using 3D printers to manufacture the blocks relate to the workability and the repeatability of the tests: the plastic blocks do not break during collapse and can be immediately reused after each test, as they are fixed with a gum layer - not fresh mortar. Although no specific prototype was targeted, a geometric scaling factor between 5 and 10 can be assumed, in accordance with relevant studies in the literature. The vault was built according to two support conditions. The first (Configuration 1) uses four fixed supports, while the second (Configuration 2) employs two fixed supports and two one-way moveable carriages equipped with lateral springs. Different lateral confinement levels along the four lateral arches (wooden panels, Plexiglas panels, cut Plexiglas panels, no panels) were also considered. Random signal tests of variable amplitude were carried out to shed light on the non-linear dynamic properties of the model. Harmonic inputs with different frequencies ranging between 1 Hz and 50 Hz were imposed, with increasing amplitude, along a single horizontal direction, up to collapse. A number of seismic tests using actual recorded motions were also performed.

The following conclusions were drawn from the experimental campaign:

1. The presence of the gum layer - essential for the rapid reconstruction of the model following collapse - has a strong influence on the global behaviour of the vault and seems to govern dynamic response, especially for low-frequency, high-acceleration harmonic inputs. The experimental observations revealed a tendency to activate different stiffness (and “effective”

natural frequencies) for each PTA level, which indicates a strongly non-linear behaviour.

2. For the aforementioned geometric scaling factor of about 5 to 10 and in light of Housner's rocking model, dynamic time is scaled by a factor of roughly 2 to 3. However, the physical modelling relative to a real vault is imperfect, since stress similitude is not preserved (e.g. the elastic moduli of the materials are not faithfully scaled). Eventually, this violation is of minor importance as sliding/rocking behaviour prevails close to failure and the associated response is less affected by stress-strain laws.
3. The effective fundamental frequency and damping of the vault naturally decreases and increases, respectively, with increasing acceleration.
4. The dynamic amplification of the vault model is mainly influenced by the lateral confinement level: the stronger the confinement, the larger the amplification factor.
5. All other conditions being equal, Configuration 2 (differential horizontal "in-plane shear" displacements at the supports through two springs) reaches the collapse condition for a lower PTA than Configuration 1. This underlines that the pseudo-static response of the vault induced by imposed displacements at its springings often represents the predominant cause of damage/failure, overshadowing the dynamic response of the vault itself.
6. The analysis of cumulative displacements and the collapse PTA values indicate that the vault put together with gum-layer interfaces is not particularly susceptible to cumulative damage, possibly due to the ability of the elastic layer at the joints to return to the original configuration - in contrast to the stiff brittle mortar in real vaults (structural restoration).
7. The seismic response of the vault depends, as expected, on the critical frequency range of the earthquake input.
8. The dynamic response of the vault with no panels along the lateral arches is similar to that of a weakly confined vault through the Plexiglas panels and indicates that the corner areas close to the springings are critical both for static stability and seismic performance. This seems to be known since ancient times, since inspection of past repairs indicates that these areas were frequently strengthened to be better embedded in the surrounding vertical masonry structures.

12 Acknowledgements

The SEBESMOVA3D project (SEeismic BEhavior of Scaled MOdels of groin VAults made by 3D printers, https://sera-ta.eucentre.it/index.php/sera-ta-project-22/) was funded by European Union's Horizon 2020 research and innovation programme SERA, under grant agreement No 730900. The authors are grateful for this support. Thanks are also due to the laboratory personnel at EQUALS laboratory, University of Bristol, UK.

13 References

[1] Parisi F., Luca F., Petruzzelli F., Risi R., Chioccarelli E., Field Inspection after the May 20th and 29th 2012 Emilia-Romagna Earthquakes. Tecnical Report; 2012.
[2] Dolce M., Nicoletti M., Ammirati A., Bianconi R., Filippi L., Gorini A., Marcucci S., Palma F., Zambonelli E., Lavecchia G., De Nardis R., Brozetti F., Boncio P., Cirillo D., Romano M.A., Costa G., Gallo A., Tiberi L., Zoppè G., Suhadolc P., Ponziani F., Formica A., The Emilia Thrust Earthquake of 20 May 2012 (Northern Italy): Strong Motion and Geological Observations -Report 1-. Technical Report; 2012.
[3] Lagomarsino S., Damage assessment of churches after L'Aquila earthquake (2009). Bull Earthq Eng. vol. 10, no. 1, pp. 73–92, 2012. 2012; doi:10.1007/s10518-011-9307-x.
[4] Baker J.F., A review of recent investigations into the behaviour of steel frames in the plastic range. J Inst Civ Eng. vol. 31:188, 1949.
[5] Neal B.G., Symonds P.S., The calculation of collapse loads for framed structures. (includes appendix). J Inst Civ Eng. vol. 35(1), pp. 21–40, 1950.
[6] Symonds P.S., Neal B.G., The calculation of failure loads on plane frames under arbitrary loading programmes. J Inst Civ Eng. vol. 35(1), pp. 41–61, 1950.
[7] Heyman J., The stone skeleton. Int J Solid Struct. vol. 2, 1996.
[8] Heyman J., The safety of masonry arches. Int J Solids Struct. vol. 11, 1969.
[9] Heyman J., The Stone Skeleton. (Press CCU, ed.). Cambridge: Cambridge University Press; 1995.
[10] De Lorenzis L., DeJong M., Ochesendorf J., Failure of masonry arches under impulse base motion. Earthq Eng Struct Dyn. no. June, pp. 2119–2136, 2007. doi:10.1002/eqe.
[11] Ferrario L., Alessandra M., Andreis V., Zanotti S., Riva P., Giuriani E., Behavior and retrofitting of single-leaf vaults under distributed horizontal forces. In: Structural Analysis of Historical Constructions –Jerzy Jasieńko (Ed). ; 2012.
[12] Shapiro E.E., Collapse mechanisms of small-scale unreinforced masonry vaults. Master Thesis, Massachusetts Institute of Technology, 2012. http://hdl.handle.net/1721.1/72648.
[13] Theodossopoulos D., Structural behaviour of historic masonry cross vaults. Thesis submitted for the Degree of Doctor of Philosophy, School of Civil and Enviromental Engineering, University of Edinburgh 2002.
[14] Theodossopoulos D., Sanderson J, Scott M., Strengthening Masonry Cross Vaults Damaged by Geometric Instability. In: Key Engineering Materials. vol. 624, no. January 2015, pp. 635–643. doi:10.4028/www.scientific.net/KEM.624.635.
[15] Como M., Statics of Historic Masonry Constructions. 3rd ed. Springer Series in Solid and Structural Mechanics; 2017.
[16] Milani G., Rossi M., Calderini C., Lagomarsino S., Tilting plane tests on a small-scale masonry cross vault: Experimental results and numerical simulations through a heterogeneous approach. Eng Struct. vol. 123, pp. 300–312, 2016. doi:10.1016/j.engstruct.2016.05.017.
[17] Rossi, M., Calderini, C., Lagomarsino, S., and Milani G. Seismic response of masonry vaulted structures : experimental and numerical modelling. In: 9th International Masonry Conference. 2014.
[18] Gaetani A., Seismic performance of masonry cross vaults: learning from historical developments and experimental testing. PhD Thesis,University Minho. 2016.
[19] Carfagnini C., Baraccani S., Silvestri S., Theodossopoulos D., The effects of in-plane shear displacements at the springings of Gothic cross vaults. Constr Build Mater. vol. 186, pp. 219–

232, 2018. doi:10.1016/j.conbuildmat.2018.07.055.

[20] D'Altri A.M., Castellazzi G., De Miranda S., Tralli A., Seismic-induced damage in historical masonry vaults: a case-study in the 2012 Emilia earthquake-stricken area. J Build Eng,vol. 13, no. August, pp. 224–243, 2017. doi:10.1016/j.jobe.2017.08.005.

[21] Creazza G., Saetta A., Matteazzi R., Vitaliani R., Analyses of masonry vaults: a macro approach based on three-dimensional damage model. Struct Eng, vol. 128, pp. 646–654, 2002.

[22] Van Mele T., McInerney J., DeJong M.J., Block P., Physical and Computational Discrete Modelling of Masonry Vault Collapse. Struct Anal Hist Constr. *Vols 1-3*, pp. 2552–2560, 2012.

[23] Calderini C., Lagomarsino S., Rossi M., De Canio G., Mongelli M.L., Roselli I., Shaking table tests of an arch-pillars system and design of strengthening by the use of tie-rods. Bull Earthq Eng, vol. 13, no. 1, pp. 279–297, 2015. doi:10.1007/s10518-014-9678-x.

[24] Gaetani A., Lourenço P.B., Monti G., Moroni M., Shaking table tests and numerical analyses on a scaled dry-joint arch undergoing windowed sine pulses. Bull Earthq Eng,vol. 15, no. 11, pp. 4939–4961, 2017. doi:10.1007/s10518-017-0156-0.

[25] Clemente P., Introduction to dynamics of stone arches. Earthq Eng Struct Dyn. 1998.

[26] Giamundo V., Lignola G.P., Maddaloni G., da Porto F., Prota A., Manfredi G.., Shaking table tests on a full-scale unreinforced and IMG retrofitted clay brick masonry barrel vault. Bull Earthq Eng, vol. 14, no. 6, pp. 1663–1693, 2016. doi:10.1007/s10518-016-9886-7.

[27] Williams M.S., Albuerne A., Lawson V., Yip F., Model Scale Shaking Table Tests on Masonry Barrel and Cross Vaults. Proc 15th world Conf Earthq Eng Lisbon. 2012:1-10.

[28] Lagomarsino, S., Modaressi, H., Pitilakis, K., Bosiljkov, V., Calderini, C., D'Ayala, D., Benouar, D., Cattari, S., PERPETUATE Project: The Proposal of a Performance-Based Approach to Earthquake Protection of Cultural Heritage. In: Advanced Materials Research. ; 2012.

[29] Rossi M., Calderini C., Lagomarsino S., Experimental testing of the seismic in-plane displacement capacity of masonry cross vaults through a scale model. Bull Earthq Eng, vol. 14, no. 1, pp. 261–281, 2016. doi:10.1007/s10518-015-9815-1.

[30] Foti D., Silvestri S., Baraccani S., Ivorra S., Theodossopoulos D., Vacca V., CampanellaV., Ocho Roman J.V., Cavallini L., White R., Dietz M., Mylonakis G.,Experimental tests of a groin vault in dry-bonded voussoirs under dynamic excitation. In: 17th World Conference on Earthquake Engineering, 17WCEE, 2020

[31] Foti D., Vacca V., Facchini I., DEM modeling and experimental analysis of the static behavior of a dry-joints masonry cross vaults. Constr Build Mater. vol. 170, pp. 111–120, 2018.

[32] Foti D, Lerna M, Sabbà MF, Vacca V. On the collapse behavior of a wood arch made with modular hollow blocks. WSEAS Trans Environ Dev,vol. 15, pp. 279–287, 2019.

[33] Diaferio M., Dassisti M., Foti, D., Vacca V., Analysis of a Mock-Up of a New Sustainable Easy-Assembling Modular Arch. Structures, vol. 19, pp. 309–321, 2019.

[34] Quinonez A., Zessin J., Nutzel A., Ochsendorf J., Small-scale models for testing masonry structures. Adv Mater Res. vol. 133–134, pp. 497–502, 2010. doi:10.4028/www.scientific.net/AMR.133-134.497.

[35] Fallacara G., Stereotomy - Stone Architecture and New Research. In: Presses des Ponts, ed. ; 2012.

[36] Fallacara G., Barberio M., Stereotomy 2.0: Informing the future of Digital Stereotomy. Nexus Netw Journal, a peer-reviewed J co-published Distrib by Birkhäuser/Springer-Basel. 2018.

[37] Croci G., The collapses occured in the basilica of St. Francis of Assisi and in the cathedral of Noto. Struct Anal Hist Constr II. 1998.

[38] Piermarini E., The Dynamic Behavior of the Basilica of San Francesco of Assisi. Master Thesis of Engineering, Massachusetts Institute of Technology, 2013.

[39] Cancino C., Farneth S., Garnier P., Vargas J., Webster F., Estudio de Daños a Edificaciones Históricas de Tierra Después Del Terremoto Del 15 de Agosto Del 2007 En Pisco, Perú. The Getty Conservation Institute Los Angeles; 2009.

[40] Housner G.W., The behavior of inverted pendulum structures during earthquakes. Bull Seismol Soc Am,vol. 53, no. 2, pp. 403–417, 163AD.

[41] Acikgoz S., DeJong M.J., The interaction of elasticity and rocking in flexible structures allowed to uplift. Earthquale Eng Struct Dyn. vol. 41, no. 15, p. 2177-2194, 2012.

[42] Vamvatiskos D., Cornell C.A., Incremental Dynamic Analysis. Earthq Eng Struct Dyn. vol. 31, no. 3, pp. 491–514, 2002.

[43] Baraccani S., Zauli L., Theodossopoulos D., Silvestri S., Experimental test on a fibre-reinforced scaled cross vault subjected to in-plane shear displacements at the springings. Constr Build Mater, Construction and Building Materials 265 (2020) 120305, https://doi.org/10.1016/j.conbuildmat.2020.120305.

[44] Baraccani S., Silvestri S., Gasparini G., Palermo M., Trombetti T., Silvestri E., Lancellotta R., Capra A., A Structural Analysis of the Modena Cathedral. Int J Archit Herit. vol. 10, no. 2–3, 2016. doi:10.1080/15583058.2015.1113344.

[45] Basile G., Restauri in San Francesco Ad Assisi: Il Cantiere Dell'utopia : Studi, Ricerche e Interventi Sui Dipinti Murali e Sulle Vetrate Dopo Il Sisma Del 26 Settembre 1997. Perugia, Italy: Quattroemme; 2007.

[46] Bianchini N., Mendes N., Calderini C., Candeias P.X., Rossi M., Lourenço P, Seismic response of a small-scale masonry cross vault: Experimental investigation by performing quasi-static and shake table tests, DOI: 10.21203/rs.3.rs-188815/v1, submitted to Bulletin of Earthquake Engineering, February 2021.

[47] Mylonakis G., Gazetas G.. Soil-Structure Interaction: Beneficial or Detrimental? Journal of Earthquake Engineering, vol. 4, no. 3, pp. 277-301.

14 Appendix

Table A1 summarises all tests performed and provides information regarding the sequence of tests, collapses and subsequent reconstructions. This is fundamental to deeply understand the overall experimental campaign and to frame the specific results of the single tests. It may also constitute a service table for independent researchers that aim to scrutinise further the experimental results.

Some notes: at the "table acceleration" column, values are measured by the accelerometer put on the table and the actual Root Mean Square (RMS) acceleration is reported for random white noise tests, whilst the actual Peak Table Acceleration (PTA) is reported for harmonic tests. In the "frequency" column, in general, the frequency of the applied harmonic input is reported, except for the random tests for which f_r indicates the "recorded system frequency" as obtained by analysing the acceleration output signal of the accelerometer on the keystone of the vault. Notation "Part.Col." stands for partial collapse.

Table A1: *Full list of all tests performed.*

Config.	**Test N.**	**Type of signal**	**Table Acceleration (RMS or PEAK)**	**Direction**	**Freq.**	**Damping Ratio**	**Config.**	**Test N.**	**Type of signal**	**Table Acceleration (RMS or PEAK)**	**Direction**	**Freq.**	**Damping Ratio**
			[g]		[Hz]	[%]				[g]		[Hz]	[%]
1A	1		0.03	X	f_r=*19.85*	11.13	1B	140	Random	0.03	X	f_r=*14.37*	14.22
1A	2	Random	0.03	Y	f_r=*19.18*	12.91	1B	141		0.03	Y	f_r=*13.88*	11.58
1A	3		0.09	Z	f_r=*21.63*	11.93	1B	142	Sin 10 c	0.90	X	*3*	
1A	4		0.11		1		1B	143		1.04			**Collapse**
1A	5		0.12		5		1B	144	Random	0.04	X	f_r=*11.99*	16.94
1A	6		0.12		8		1B	145		0.03	Y	f_r=*13.34*	11.33
1A	7		0.12		10		2B	146		0.04	X	f_r=*7.36*	19.13
1A	8	Sin 10 c	0.10	X	15		1B (by means of 2B)	147		0.03	Y	f_r=*13.29*	11.34
1A	9		0.10		20		2B	148	Random	0.07		f_r=*6.01*	19.81
1A	10		0.11		50		2B	149		0.14	X	f_r=*5.24*	15.89
1A	11		0.26		1		2B	150		0.18		f_r=*4.87*	24.76
1A	12		0.26		5		2B	151		0.04		f_r=*6.88*	20.50
1A	13		0.29		8		2B	152		0.11		50	
1A	14	Sin 10 c	0.29	X	10		2B	153		0.11		20	
1A	15		0.23		15		2B	154		0.10		15	
1A	16		0.25		20		2B	155		0.10		10	
1A	17		0.29		50		2B	156	Sin 10 c	0.10	X	8	
1A	18		0.51		1		2B	157		0.12		6	
1A	19	Sin 10 c	0.53	X	5		2B	158		0.11		5	
1A	20		0.54		8		2B	159		0.11		4	
1A	21		0.53		10		2B	160		0.11		3	

1A	22		0.42		15		2B	161		0.11		2	
1A	23		0.43		20		2B	162		0.11		1	
1A	24		0.52		50		2B	163	Random	0.04	X	f_r=*6.48*	25.41
1A	25		0.74		2		2B	164		0.30		50	
1A	26		0.78		5		2B	165		0.19		20	
1A	27		0.77		8		2B	166		0.24		15	
1A	28	Sin 10 c	0.78	X	10		2B	167		0.24		10	
1A	29		0.58		15		2B	168	Sin 10 c	0.24		8	
1A	30		0.63		20		2B	169		0.28	X	6	
1A	31		1.11		2	**Collapse**	2B	170		0.25		5	
1A	32	Random	0.03	X	f_r=*15.79*	12.4	2B	171		0.25		4	
1A	33		0.65		15		2B	172		0.25		3	
1A	34		0.80		10		2B	173		0.26		2	**Part.Col.**
1A	35		0.83		8		2B	174	Sin 30 c	0.25		2	**Collapse**
1A	36	Sin 10 c	0.81	X	5		2B	175		0.04	X	f_r=*7.07*	17.49
1A	37		0.79		2		1B (by means of 2B)	176	Random	0.03	Y	f_r=*13.86*	9.44
1A	38		0.70		15		2B	177	Sin 10 c	0.07		3	
1A	39		0.86		10		2B	178	Random	0.04		f_r=*7.04*	17.15
1A	40	Sin 10 c	0.87	X	8		2B	179	Sin 10 c	0.12		3	
1A	41		0.87		5		2B	180	Random	0.04		f_r=*6.87*	16.93
1A	42		0.84		2		2B	181	Sin 10 c	0.16		3	
1A	43		0.73		15		2B	182	Random	0.03		f_r=*5.66*	20.86
1A	44		0.94		10		2B	183	Sin 10 c	0.19		3	
1A	45	Sin 10 c	0.92	X	8		2B	184	Random	0.04		f_r=*6.42*	22.81
1A	46		0.93		5		2B	185	Sin 10 c	0.24		3	
1A	47		0.91		2		2B	186	Random	0.04	X	f_r=*6.23*	23.25
1A	48		0.79		15		2B	187		0.29			
1A	49		0.99		10		2B	188		0.35			
1A	50	Sin 10 c	0.99	X	8		2B	189		0.40			
1A	51		0.99		5		2B	190	Sin 10 c	0.46			
1A	52		1.01		2	**Collapse**	2B	191		0.51		3	**Part.Col.**
1A	53	Random	0.04	X	f_r=*15.78*	12.36	2B	192		0.61			**Part.Col.**
1A	54	Modena eqke	0.36	X			2B	193		0.76			**Part.Col.**
1A	55	Random	0.02	X	f_r=*15.39*	12.76	2B	194	Sin 100 c	1.01			**Collapse**
1A	56	Mirandola eqke	0.25				2B	195		0.04	X	f_r=*7.24*	15.69
1A	57		0.36				1B (by means of 2B)	196	Random	0.04	Y	f_r=*12.65*	10.78
1A	58	El Centro eqke	0.69	X			2B	197	Sin 500 c	0.35	X	3	
1A	59		0.89				2B	198		0.20		3	
1A	60		0.70				Repaired Vault						
1A	61		1.10	Y	5		2B	199		0.04	X	f_r=*6.97*	4.51
1A	62	Sin 10 c	1.34	Y	5		1B (by means of 2B)	200	Random	0.04	Y	f_r=*13.71*	9.57
1A	63		1.59	Y	5	**Part.Col.**	2B	201	Sin 500 c	0.27	X	2.5	
1A	64	Random	0.03	X	f_r=*17.16*	11.18	2B	202		0.19		2.5	

1A	65		0.02	Y	f_r=17.20	9.68	2B	203		0.21		2	**Collapse**
1A	66		0.05		f_r=15.05	13.14	2C	204		0.04	X	f_r=6.29	13.08
1A	67		0.13		f_r=12.46	18.93	1C (by means of 2C)	205		0.04	Y	f_r=10.54	10.50
1A	68		0.22		f_r=10.26	17.15	2C	206		0.07	X	f_r=5.40	13.66
1A	69		0.30	X	f_r=9.46	22.69	1C (by means of 2C)	207		0.06	Y	f_r=9.97	10.48
1A	70		0.38		f_r=8.78	28.91	2C	208		0.12	X	f_r=4.75	17.36
1A	71		0.47		f_r=7.69	27.02	1C (by means of 2C)	209	Random	0.12	Y	f_r=8.82	13.31
1A	72		0.57		f_r=6.94	50.54	2C	210		0.18	X	f_r=3.90	23.89
1B	73		0.04	X	f_r=14.95	11.09	1C (by means of 2C)	211		0.16	Y	f_r=8.31	13.86
1B	74		0.03	Y	f_r=14.84	11.17	2C	212		0.04	X	f_r=6.47	16.22
1B	75	Random	0.07		f_r=13.46	13.65	1C (by means of 2C)	213		0.04	Y	f_r=10.78	10.22
1B	76		0.14	X	f_r=11.58	17.51	2C	214		0.10		50	
1B	77		0.22		f_r=10.13	20.09	2C	215		0.10		20	
1B	78		0.04		f_r=14.83	11.78	2C	216		0.10		15	
1B	79		0.31		50		2C	217		0.10		10	
1B	80		0.17		20		2C	218		0.10		8	
1B	81		0.20		15		2C	219	Sin 10 c	0.11	X	6	
1B	82		0.24		10		2C	220		0.11		5	
1B	83	Sin 10 c	0.25	X	8		2C	221		0.11		4	
1B	84		0.26		5		2C	222		0.11		3	
1B	85		0.25		3		2C	223		0.11		2	
1B	86		0.26		2		2C	224		0.11		1	
1B	87		0.44		1		2C	225	Random	0.04	X	f_r=6.45	20.72
1B	88	Random	0.04	X	f_r=15.02	13.25	2C	226		0.29		50	
1B	89		0.53		50		2C	227		0.20		20	
1B	90		0.40		20		2C	228		0.25		15	
1B	91		0.42		15		2C	229		0.25		10	
1B	92		0.48		10		2C	230	Sin 10 c	0.24		8	
1B	93	Sin 10 c	0.49	X	8		2C	231		0.27	X	6	
1B	94		0.52		5		2C	232		0.25		5	
1B	95		0.51		3		2C	233		0.25		4	
1B	96		0.50		2		2C	234		0.25		3	
1B	97		0.50		1		2C	235		0.26		2	**Part.Col.**
1B	98	Random	0.04	X	f_r=14.49	14.20	2C	236	Sin 30 c	0.26		2	**Collapse**
1B	99		0.84		50		1D (by means of 2D)	237		0.05	Y	f_r=9.40	9.49
1B	100	Sin 10 c	0.66	X	20		2D	238	Random	0.04	X	f_r=4.76	48.79
1B	101		0.65		15		1D (by means of 2D)	239		0.07	Y	f_r=8.69	8.89
1B	102		0.78		10		2D	240		0.07	X	f_r=4.65	17.06

1B	103		0.75		8		1D (by means of 2D)	241		0.12	Y	$f_r=7.62$	11.91
1B	104		0.77		5		2D	242		0.13	X	$f_r=3.71$	15.02
1B	105		0.76		3		1D (by means of 2D)	243		0.17	Y	$f_r=6.65$	10.32
1B	106		0.73		2		2D	244		0.18	X	$f_r=3.98$	17.93
1B	107	Random	0.04	X	$f_r=13.83$	14.93	1D (by means of 2D)	245		0.15	Y	5	
1B	108	Sin 100 c	0.77	X	5		2D	246		0.11	X	5	
1B	109		0.76		3		1D (by means of 2D)	247	Sin 10 c	0.14	Y	3	
1B	110	Random	0.03	X	$f_r=15.16$	14.58	2D	248		0.10	X	3	
1B	111		0.21		$f_r=10.51$	36.99	1D (by means of 2D)	249		0.14	Y	2	
1B	112		0.76				2D	250		0.11	X	2	
1B	113		0.76				1D (by means of 2D)	251	Random	0.04	Y	$f_r=10.12$	8.93
1B	114		0.76				2D	252		0.04	X	$f_r=5.57$	12.91
1B	115	Sin 100 c	0.76	X	5		1D (by means of 2D)	253	Sin 10 c	0.08	Y	3	
1B	116		0.77				2D	254		0.06	X	3	
1B	117		0.76				1D (by means of 2D)	255	Random	0.04	Y	$f_r=10.16$	8.83
1B	118		0.76			**Collapse**	2D	256	Random	0.04	X	$f_r=5.41$	9.23
1B	119	Random	0.04	X	$f_r=14.77$	11.63	1D (by means of 2D)	257	Sin 10 c	0.13	Y	3	
1B	120		0.03	Y	$f_r=14.22$	11.25	2D	258		0.11	X	3	**Part.Col.**
1B	121	Sin 10 c	0.11	X	3		1D (by means of 2D)	259	Random	0.04	Y	$f_r=9.78$	9.27
1B	122	Random	0.04	X	$f_r=14.90$	11.50	2D	260		0.04	X	$f_r=5.66$	9.07
1B	123	Sin 10 c	0.20	X	3		2D	261	Sin 10 c	0.15	X	3	**Part.Col.**
1B	124	Random	0.04	X	$f_r=14.85$	11.71	2D	262		0.20			**Part.Col.**
1B	125	Sin 10 c	0.29	X	3		2D	263		0.25			**Part.Col.**
1B	126	Random	0.04	X	$f_r=14.87$	11.01	2D	264		0.28			**Part.Col.**
1B	127	Sin 10 c	0.40	X	3		2D	265		0.34			**Part.Col.**
1B	128	Random	0.04	X	$f_r=14.62$	12.14	2D	266		0.39			**Collapse**
1B	129	Sin 10 c	0.51	X	3								
1B	130	Random	0.04	X	$f_r=14.40$	12.03							
1B	131	Sin 10 c	0.60	X	3								
1B	132	Random	0.04	X	$f_r=14.22$	12.31							
1B	133	Sin 10 c	0.69	X	3								
1B	134	Random	0.04	X	$f_r=14.23$	13.29							
1B	135	Sin 10 c	0.81	X	3								
1B	136	Random	0.04	X	$f_r=13.84$	13.06							
1B	137	Sin 10 c	0.92	X	3								

1B	138	Random	0.04	X	*f_r=12.63*	13.71							
1B	139	Sin 10 c	1.02	X	3	**Collapse**							